The Astrophysical Journal, 900:148 (10pp), 2020 September 10 https://doi.org/10.3847/1538-4357/abad31

Chandra Observations of Candidate Subparsec Binary Supermassive Black Holes

M. Lynne Saade[1], Daniel Stern[2], Murray Brightman[3], Zoltán Haiman[4], S. G. Djorgovski[3], Daniel D'Orazio[5], K. E. S. Ford[6,7,8], Matthew J. Graham[3], Hyunsung D. Jun[9], Ralph P. Kraft[10], Barry McKernan[6,7,8], Alexei Vikhlinin[10], and Dominic J. Walton[11]

[1] Department of Physics and Astronomy, University of California, 475 Portola Plaza, Los Angeles, CA 90095, USA; mlsaade@astro.ucla.edu
[2] Jet Propulsion Laboratory, California Institute of Technology, 4800 Oak Grove Drive, Pasadena, CA 91109, USA
[3] Cahill Center for Astronomy and Astrophysics, California Institute of Technology, 1216 E. California Boulevard, Pasadena, CA 91125, USA
[4] Department of Astronomy, Columbia University, New York, NY 10027, USA
[5] Department of Astronomy, Harvard University, 60 Garden Street, Cambridge, MA 02138, USA
[6] Department of Astrophysics, American Museum of Natural History, Central Park West at 79th Street, New York, NY 10024, USA
[7] Department of Science, Borough of Manhattan Community College, City University of New York, New York, NY 10007, USA
[8] Physics Program, The Graduate Center, City University of New York, New York, NY 10016, USA
[9] School of Physics, Korea Institute for Advanced Study, 85 Hoegiro, Dongdaemun-gu, Seoul 02455, Republic of Korea
[10] Harvard-Smithsonian Center for Astrophysics, 60 Garden Street, Cambridge, MA 02138, USA
[11] Institute of Astronomy, University of Cambridge, Madingley Road, Cambridge CB3 0HA, UK
Received 2020 February 18; revised 2020 July 22; accepted 2020 August 5; published 2020 September 11

Abstract

We present analysis of Chandra X-ray observations of seven quasars that were identified as candidate subparsec binary supermassive black hole (SMBH) systems in the Catalina Real-Time Transient Survey based on the apparent periodicity in their optical light curves. Simulations predict that close-separation accreting SMBH binaries will have different X-ray spectra than single accreting SMBHs, including harder or softer X-ray spectra, ripple-like profiles in the Fe K-α line, and distinct peaks in the spectrum due to the separation of the accretion disk into a circumbinary disk and mini disks around each SMBH. We obtained Chandra observations to test these models and assess whether these quasars could contain binary SMBHs. We instead find that the quasar spectra are all well fit by simple absorbed power-law models, with the rest-frame 2–10 keV photon indices, Γ, and the X-ray-to-optical power slopes, $\alpha_{\rm OX}$, indistinguishable from those of the larger quasar population. This may indicate that these seven quasars are not truly subparsec binary SMBH systems, or it may simply reflect that our sample size was too small to robustly detect any differences. Alternatively, the X-ray spectral changes might only be evident at energies higher than probed by Chandra. Given the available models and current data, no firm conclusions are drawn. These observations will help motivate and direct further work on theoretical models of binary SMBH systems, such as modeling systems with thinner accretion disks and larger binary separations.

Unified Astronomy Thesaurus concepts: Quasars (1319); Supermassive black holes (1663); Active galactic nuclei (16); Active galaxies (17); X-ray active galactic nuclei (2035)

1. Introduction

Supermassive black holes (SMBHs) are believed to exist in the nuclei of all large galaxies. When galaxies merge, their respective SMBHs generally pair up to form binaries. The SMBH binary separation will then slowly shrink due to dynamical friction and multibody interactions in asymmetric stellar distributions, as well as due to gas dynamics (Berczik et al. 2006; Mayer et al. 2007; Gualandris et al. 2017). Multibody interactions with other SMBHs can also be relevant (Ryu et al. 2018). Once the binary reaches subparsec scales, the SMBHs can spiral together and merge on timescales shorter than the age of the universe (Begelman et al. 1980). In the final months or years, corresponding to the final 100–1000 orbits before merger, binary SMBHs become strong gravitational wave sources that should be detectable by pulsar timing arrays or future observatories such as the Laser Interferometer Space Antenna (Amaro-Seoane et al. 2017). Close-separation binary SMBHs are therefore important for a range of astrophysical studies, from black hole growth, to active galactic nucleus (AGN) triggering, to gravitational wave physics. However, few such systems have been conclusively identified to date, and theoretical predictions of their multiwavelength properties vary greatly. In the following, we first review candidate binary SMBHs in the literature (Section 1.1), followed by a review of proposed observational signatures of such systems based on theoretical work (Section 1.2). We then discuss the motivation behind the work presented here (Section 1.3).

1.1. Candidate Binary SMBHs in the Literature

The first reported candidate subparsec binary SMBH was the blazar OJ 287, which displays quasiperiodic optical outbursts every 12 years that could be explained by a binary SMBH slowly decaying under the effects of gravitational radiation (Lehto & Valtonen 1996). The binary explanation involves a $1.8 \times 10^{10} M_{\odot}$ primary (Valtonen et al. 2008) with a $1.4 \times 10^{8} M_{\odot}$ secondary (Valtonen et al. 2012) that impacts the primary's accretion disk nearly once per decade. With an optical light curve spanning over 120 yr (Valtonen et al. 2012), OJ 287 is considered one of the strongest binary SMBH candidates to date.

Additional strong candidate SMBH merger precursors come from systems where multiple, well-separated AGNs are imaged in the same galaxy, such as the two Chandra-detected X-ray AGNs in NGC 6420 (Komossa et al. 2003), other dual X-ray sources (e.g., Koss et al. 2011, 2012; Comerford et al. 2015; Satyapal et al. 2017; Hou et al. 2019; Pfeifle et al. 2019a, 2019b; Foord et al. 2020), dual radio sources (e.g., Rodriguez et al. 2006; Fu et al. 2011, 2015; Müller-Sánchez

et al. 2015; Kharb et al. 2017; Rubinur et al. 2019), and dual optical sources (e.g., Liu et al. 2011; Comerford et al. 2012, 2013; Goulding et al. 2019). For a recent review paper on dual and binary AGNs, see De Rosa et al. (2020). As reliably distinguishing two AGNs from each other requires the AGN to be well separated, the dual AGNs identified through this method have generally had separations greater than 1 kpc. For many years, the closest example of a merging SMBH system with multiple AGNs detected in imaging was the pair of flat-spectrum radio sources in 0402+379, separated by 7.3 pc (Rodriguez et al. 2006). Recently, this has been superseded by a 0.35 pc pair of radio cores in NGC 7674 imaged at 15 GHz using very long baseline interferometry (VLBI; Kharb et al. 2017), and it is possible in the near future that subparsec binaries will be resolved with more advanced VLBI like the Event Horizon Telescope (D'Orazio & Loeb 2018).

Unusual radio morphologies can also identify candidate merging SMBH systems because jet precession is a well-established consequence of binary black hole systems (e.g., Gower et al. 1982). VLBI observations have revealed several examples of AGNs with jet morphology suggestive of precession, such as S5 1928+738 (Kun et al. 2014), 3C 345 (Lobanov & Roland 2005), and BL Lacertae (Caproni et al. 2013). Tsai et al. (2013) and Krause et al. (2019) present additional examples based on Australian Telescope Compact Array, Very Large Array, and Multi-Element Radio Linked Interferometer Network observations. However, these binary SMBH candidates based on jet morphology are considered controversial as Kelvin–Helmholtz instabilities can also mimic the warping of jets due to precession (e.g., Romero 1995; Lobanov & Zensus 2001).

More recently, there have been attempts to identify candidate binary SMBHs based on broad emission-line profiles, under the assumption that a binary SMBH would modify the lines in a manner similar to a binary star system. Eracleous et al. (2012) carried out the first systematic search for quasars with broad-line peaks substantially shifted from their nominal wavelengths (by thousands of km s^{-1}). They identified 88 such quasars in the Sloan Digital Sky Survey (SDSS), with 14 showing statistically significant changes in Hβ peak velocities. Further candidates from SDSS have been reported based on Mg II and Hβ emission lines (e.g., Ju et al. 2013; Shen et al. 2013; Liu et al. 2014; Guo et al. 2019). However, it might not be possible to identify highly subparsec binaries (e.g., $\leqslant$0.01 pc separation) with spectroscopic techniques, as the broad-line region (BLR) would be far larger than the orbit of either SMBH, making it potentially insensitive to their movements (Shen & Loeb 2010). Furthermore, several phenomena associated with isolated SMBHs could produce velocity offsets claimed as evidence of binary SMBHs, such as asymmetric reverberation-induced velocity shifts (Barth et al. 2016) and unusual BLR geometries (Liu et al. 2016). Wang et al. (2017) updated the analysis of the Ju et al. (2013) candidates, as well as observed 1438 more objects with a baseline of 8 yr, and found only one candidate with an outlying velocity shift. Subject to these caveats, Li et al. (2016) reported a candidate close, centiparsec (0.018 pc) SMBH binary in the galaxy NGC 5548 based on four decades of spectroscopic monitoring.

Binary SMBH systems can also produce cutoffs or notches in their continuum spectra, evident at rest-frame ultraviolet wavelengths, due to the presence of a secondary black hole truncating or clearing a gap or cavity in the circumbinary disk. Guo et al. (2020) recently presented a comprehensive analysis of the spectral energy distributions (SEDs) of ~150 published candidate periodically variable quasars but found that the candidate periodic quasars are similar to the control sample matched in redshift and luminosity.

Perhaps the most promising way to identify highly subparsec binary SMBHs is through periodicity in AGN light curves. After OJ 287, the first examples of such objects were found in the Catalina Real-Time Transient Survey (CRTS; Drake et al. 2009). Graham et al. (2015a) reported the first such example, PG 1302–102, and Graham et al. (2015b) presented a sample of 111 candidate periodic quasars selected from a systematic analysis of 243,500 quasars with well-sampled CRTS light curves.[12] Notably, PG 1302–102 shows the same periodicity in ultraviolet (D'Orazio et al. 2015b) and mid-IR wavelengths (Jun et al. 2015), as well as in the position angle of its radio jet (Qian et al. 2018). D'Orazio et al. (2015b) showed that the periodicity of PG 1302–102 could be well explained by a binary SMBH with a mass ratio of $\leqslant$0.3 separated by 0.007–0.017 pc (i.e., 1400–3500 au). Relativistic Doppler boosting and beaming of emission from the secondary SMBH's accretion disk as it orbits a more massive ($\geqslant 10^{9.1}\,M_{\odot}$) primary create the variations observed in the light curve. Liu et al. (2018) argued that including data from the All-Automated Sky Survey for Supernovae weakened the case for true periodicity in PG 1302–102, though Xin et al. (2020) reported on nine additional epochs of simultaneous ultraviolet and optical Swift observations, finding light curves roughly consistent with the expected trends for the binary model.

Since the landmark study from Graham et al. (2015b), several other instances of claimed periodicity have been reported in quasar optical light curves, including examples from the optical photometric databases of Pan-STARRS (Liu et al. 2019) and the Palomar Transient Factory (Charisi et al. 2016; Dorn-Wallenstein et al. 2017). At higher energies, there have been reports of quasiperiodicity in the gamma-ray light curves of several blazars (Sandrinelli et al. 2016), suggestive of SMBH binaries akin to OJ 287, and claims of modular Swift-BAT and Swift-XRT light curves in a local Seyfert galaxy (Severgnini et al. 2018). However, concerns with the statistical analyses have been common, including noting the importance of including "red noise" stochastic quasar variability when calculating the false-alarm probability (Vaughan et al. 2016), as well as a proper consideration of the look-elsewhere effect (Barth & Stern 2018). While some studies have accounted for these effects in full (e.g., Graham et al. 2015b; Charisi et al. 2016), the form of the red noise has sometimes been questioned. For example, Charisi et al. (2016) adopted a damped random walk (DRW) model with Gaussian red noise. M. J. Graham et al. (2020, in preparation) presents a more in-depth analysis of these issues, as well as updates the Graham

[12] Note that the newly identified periodic quasars are selected on the basis of sinusoidal variability, which is quite distinct from the regular flaring activity seen in OJ 287. The sinusoidal light curves are believed to be due to two SMBHs sharing a single circumbinary accretion disk, which naturally leads to the lower-mass black hole having a higher accretion rate and thus the black holes rapidly becoming of near-equal mass. OJ 287, on the other hand, has a small secondary SMBH plunging through the accretion disk of a significantly (~100×) more massive primary twice per orbit (Dey et al. 2018). Therefore, many of the tests for a binary SMBH described below (Section 1.2), and, in particular, tests based on X-ray spectral analysis, are not relevant for OJ 287 despite the significant X-ray observations that exist for this system (e.g., Marscher & Jorstad 2011; Kushwaha et al. 2018; Pal et al. 2020).

et al. (2015b) sample with several more years of photometric monitoring.

1.2. Predicted Observational Signatures of Binary SMBHs

Theoretical models predict a variety of features to be present in accreting binary SMBHs. The two black holes are surrounded by a circumbinary disk, from which accretion streams feed onto mini disks surrounding each individual black hole. In the interior of the circumbinary disk, a cavity is cleared out by tidal torques from the binary (Artymowicz & Lubow 1994). Figure 8 in d'Ascoli et al. (2018) and Figure 3 in Farris et al. (2014) both provide good illustrations of these features.

Despite the presence of the cavity, the accretion rate onto the SMBHs is not lower than for a single SMBH (D'Orazio et al. 2013) and can temporarily exceed that for a single SMBH (Rafikov 2016). The total luminosity of the system is also not lower than that for a single SMBH (Farris et al. 2015b). For highly unequal mass binaries expected to form as a result of hierarchical galaxy formation (e.g., Volonteri et al. 2003), most of the luminosity arises from accretion onto the secondary black hole (Farris et al. 2014; Duffell et al. 2019).

Because accretion is able to proceed in a binary SMBH system as efficiently as with a single SMBH, binary SMBHs should still be able to launch jets. It is well established that jets will precess under the influence of a black hole binary, creating a jet morphology that is helical on a conical surface (Gower et al. 1982) or wiggled and knotted (Kaastra & Roos 1992). The Doppler shift in the synchrotron radiation of the jet will vary periodically due to the precession of the jet, creating periodicity in the radio light curve (Kun et al. 2014).

Multiple mechanisms might also cause the accretion onto binary SMBHs to be periodic as well. D'Orazio et al. (2013) discuss oscillations in accretion rate created by hydrodynamic interactions of the accretion streams with an overdense lump at the inner edge of the circumbinary disk (see also Farris et al. 2014; Shi & Krolik 2015). The resulting periodicity in emission depends on whether emission arises primarily from the circumbinary disk or from the mini disks—with implications for the soft versus hard X-ray light curve as well (Tang et al. 2018). Doppler boosts are another possible source of periodic behavior (e.g., D'Orazio et al. 2015b). For a binary where the primary and secondary have equal mass, $M_1 = M_2$, accretion rate oscillations will dominate over Doppler boost oscillations (Tang et al. 2018). However, hydrodynamical modulations decline in magnitude with decreasing mass ratio, $q \equiv M_2/M_1$, such that for $q \leqslant 0.05$, Doppler effects dominate the periodicity (D'Orazio et al. 2013; Farris et al. 2014; Duffell et al. 2019). One last additional source of potential periodic behavior is self-lensing of the accretion flow of one SMBH by the gravitational field of the other (Haiman 2017; D'Orazio & Stefano 2018). It is worth distinguishing the relative shapes these modulations introduce onto the light curve, varying from quasi-sinusoidal (Doppler), to bursty (hydrodynamic), to repeating sharp spikes (self-lensing). Current searches for periodic behavior in AGN light curves may only be able to detect the first of these shapes.

In addition to periodicity, potential spectral signatures of binary SMBHs have been considered in the literature. In the UV/optical portion of the electromagnetic spectrum, Roedig et al. (2014) argued that the central cavity cleared by the binary would generate a deep notch in the thermal continuum. In contrast, Farris et al. (2015a) and d'Ascoli et al. (2018) did not recover the notch, finding that the accretion streams compensate for this gap. Nguyen & Bogdanovic (2016) generated a database of Hβ emission-line profiles for subparsec binary SMBHs assuming both SMBHs possess mini disks and illuminate the circumbinary disk. Some of the line profiles generated were highly complex and time variable, including multiple peaks, but they were also highly dependent on the semimajor axis of the binary as well as on the alignment between the mini disks and the observer. Further work by Nguyen et al. (2019) revealed that including the effects of accretion disk winds eliminated the more complex line profiles. This recent work therefore argued that emission-line profiles on their own cannot be used to confirm an SMBH binary.

In the X-rays, potential sources of emission in a binary SMBH are the circumbinary disk (Tang et al. 2018), hot spots where the accretion streams from the circumbinary disk collide with the mini disks around each SMBH (Roedig et al. 2014), and the mini disks themselves (Farris et al. 2015b). Roedig et al. (2014) predicted that a binary SMBH would have a substantially harder X-ray spectrum than a single SMBH due to thermal emission from the hot spots, with Wien tail emission causing a peak in the spectrum at $\gtrsim$100 keV. Ryan & McFayden (2017) found a similar hardening of the X-ray spectrum of binary SMBHs compared to a Novikov–Thorne relativistic thin-disk model of an isolated accreting SMBH. However, their hardening takes place at lower energies, at $\gtrsim$10 keV. Farris et al. (2015b) predicted that the X-ray spectrum of a binary SMBH will be distinctly harder than a single SMBH that results from a merger. Tang et al. (2018) modeled close binaries up until merger and predicted that the Doppler effect will suppress 1–20 keV emission while enhancing higher-energy emission during the binary phase. They predicted two thermal peaks in the X-ray spectrum, one from the circumbinary disk at $\approx$1 keV and another from the mini disks at $\approx$20 keV, with a shallow notch between them. In their simulations of the X-ray spectrum of close binary SMBH systems, d'Ascoli et al. (2018) only recovered a single peak at $\approx$20 keV, due to Compton reflection by cold, optically thick matter in the vicinity of the central engine, as commonly seen in isolated SMBH systems (e.g., George & Fabian 1991), while emission in the soft X-rays was dominated by the thermal Wien tail from the mini disks. Their hard X-ray emission was a similar fraction of the total luminosity as that in a single SMBH system, whereas the thermal soft X-ray emission component was more pronounced than in a single SMBH system, though overall they point out their binary SMBH spectrum is more modestly different from a single SMBH spectrum compared to previous models in the literature. Thus, while many results indicate that binary SMBHs should have enhanced X-ray emission relative to single SMBH systems, there is a wide range in the predicted energy at which these enhancements would be seen, ranging from relatively low rest-frame energies of $\sim$1 keV (e.g., Farris et al. 2015b) to energies more than two orders of magnitude higher (e.g., Roedig et al. 2014). This raises the possibility of binary SMBH systems having dramatically different X-ray spectral indices or ratios of optical-to-X-ray luminosity than single SMBH systems, which we investigate in Sections 3.1 and 3.2.

McKernan et al. (2013) also predicted unique patterns of Fe K-α X-ray spectral lines due to the clearing of the central circumbinary disk by the inward migrating secondary. The

broad Fe K-α line profile becomes ripple shaped due to the presence of an annular gap, with dips in both the red and blue wings of the profile. The energy of these dips depends on the orbital separation. If an inner cavity is cleared in the circumbinary disk, the wings of the broad-line profile are suppressed, and if gas piles up at the outer edge of the cavity, double peaks will appear in the broad-line profile. McKernan et al. (2013) also modeled the effects of having both the primary and secondary accrete, which creates a secondary broad-line component that oscillates on an orbital timescale across the Fe K-α line of the primary. This opens the exciting possibility of spectroscopically detecting very compact binary SMBHs through Doppler shifts in the Fe K-α lines.

It should be noted that models in the literature have only considered binaries with close separations less than a few hundred gravitational radii. We discuss the implications of this further in Section 4.1.

1.3. Motivation for This Work

We present the first X-ray spectra for a sample of candidate subparsec binary SMBHs. Foord et al. (2017) presented a related analysis of a single candidate binary SMBH system (see Section 4.1). X-rays probe regions of an AGN closer to the central engine than do optical and ultraviolet emission, and theoretical work suggests that the unique high-energy emission of binary SMBHs could confirm the nature of such systems, as well as provide great promise for probing the compact inner regions where a subparsec binary SMBH would be located. However, the wide range of high-energy predictions leaves significant uncertainty in distinguishing features of binary SMBHs. For example, Tang et al. (2018) and d'Ascoli et al. (2018) have very different predictions for modeled binaries of similar separation, with the former predicting two peaks in the X-ray spectrum and the latter predicting a single peak. Indeed, no simulation to date has predicted a spectrum with correct and self-consistent thermodynamics, and the results, including the overall scaling of the spectrum (e.g., photon energy, emerging luminosity), are therefore subject to very large uncertainty. This uncertainty reflects the range of different ad hoc thermodynamical assumptions in different papers. We therefore crafted our program to provide a first set of observational results to motivate future models, with the goal of searching for any substantial differences in the spectra of candidate binary SMBHs. Specifically, we sought to observe the maximal number of sources in the minimal amount of observing time. While emission lines like Fe K-α are another promising way to use X-ray spectra to confirm and study close binary SMBH systems (McKernan et al. 2013), the requirements for sufficient detections were beyond the scope of this observational program.

The X-ray data come from a combination of guest observer (GO) and guaranteed time observations (GTO) with the Chandra X-ray Observatory. The rest of the paper is structured as follows: Section 2 presents the sample selection and X-ray observations; Section 3 discusses the properties of the sample; Section 4 discusses the results, summarizes our conclusions, and discusses possibilities for future work. Throughout, we adopt the concordance cosmology, $\Omega_{\rm M} = 0.3$, $\Omega_{\Lambda} = 0.7$ and $H_0 = 70\ {\rm km\ s^{-1}\ Mpc^{-1}}$.

2. Sample and X-Ray Data

2.1. Sample Selection and Chandra Observations

We selected for observation candidate periodic quasars from Graham et al. (2015b). In order to ensure high-quality X-ray spectra for this first investigation of a sample of candidate subparsec binary SMBH systems in a reasonable observing program (e.g., $\gtrsim$1000 counts in $\lesssim$10 ks, per source), we cross-correlated the 111 sources in Graham et al. (2015b) with the ROSAT All-Sky Survey Bright Source Catalog (Voges et al. 1999). Using an 18″ matching radius (approximately twice the astrometric uncertainty of that survey), nine sources were found to have ROSAT detections. PG 1302–102, the first candidate subparsec binary SMBH identified from a periodic optical light curve (Graham et al. 2015a), was awarded Chandra GTO time in Cycle 18 (P.I. R. Kraft; Obs IDs 19745–19746). Another six sources were awarded GO time in the same cycle (P.I. D. Stern; Obs IDs 19525–19530). Table 1 presents the basic properties of the target sample and details of the Chandra observations. The sources range from relatively local (e.g., Mrk 504 at $z = 0.036$; $\sim$160 Mpc) to $z > 1$. Chandra exposure times range from 2.7 to 15.9 ks. The sources were all observed using the ACIS-S instrument.

2.2. Chandra Data Analysis

We extracted the Chandra spectra using the standard Chandra software package CIAO (version 4.10) with the latest calibration files from CALDB (version 4.8.0). We extracted spectra using the default spectral grouping carried out by CIAO `specextract`, where the spectrum is grouped with a minimum of 15 counts per bin. The spectra were extracted in circular source regions with 2″ radius, with backgrounds measured in source-free annular regions centered on the targets of inner radius 10″ and outer radius 20″. The spectra were analyzed using XSPEC with the background subtracted and the χ^2 statistic for fitting. We fit each source to a simple power law, adopting the appropriate Galactic absorption from the National Radio Astronomy Observatory (Dickey & Lockman 1991). We also investigated including an additional absorption component at the source redshift, but the resulting absorption columns were negligible and the changes in χ^2 did not justify this choice of fit. The one exception was 2MASSi J0411469+132416. However, the statistical fitting favored physically implausible values $\Gamma > 5$ and $N_{\rm H} \sim 10^{23}\ {\rm cm^{-2}}$, which were particularly unlikely values given the shape of the 2MASSi J0411469 +132416 X-ray spectrum and the broad Balmer lines in its optical spectrum. Therefore, only Galactic absorption was ultimately included in the final fits for all sources. We did not detect any Fe K-α lines, which is typical for unobscured AGNs with fewer than $\approx 10^5$ counts (de La Calle Pérez et al. 2010). Table 2 presents the results of the spectral fitting, and Figure A1 shows the Chandra X-ray spectra from this study.

3. Properties of Sample

3.1. Black Hole Binary and Active Galaxy Properties

We recovered black hole masses for each quasar from Graham et al. (2015b), with the exceptions of Mrk 504 and 4C +50.43 which lacked masses in that paper. For Mrk 504, we use the mass from Ho et al. (2008), while for 4C +50.43, we derived a mass from Palomar optical spectra obtained in 2019 September using the relations in Jun et al. (2015).

Table 1
Target Sample and Chandra Observation Details

Object	R.A., Decl. (J2000)	z	Obs. Date	Exposure (ks)
2MASSi J0411469+132416	04:11:46.90, +13:24:16.0	0.277	2017 Mar 26	2.7
2MASXi J0729087+400836	07:29:08.71, +40:08:36.6	0.074	2017 Apr 28	7.6
RBS 874	10:30:24.95, +55:16:22.7	0.435	2017 Sep 4	15.4
PG 1302–102	13:05:33.01, −10:33:19.4	0.278	2016 Dec 14	10.3
FBQS J163302.6+234928	16:33:02.66, +23:49:28.5	0.821	2017 May 19	7.4
Mrk 504	17:01:07.76, +29:24:25.0	0.036	2017 Jun 21	5.1
4C +50.43	17:31:03.60, +50:07:34.0	1.070	2018 Apr 17	15.9

Table 2
X-Ray Properties of the Sample

Object	Counts[a]	Γ[b]	f_{2-10}[c]	χ^2/DOF	α_{OX}
2MASSi J0411469 +132416	218	$2.29^{+0.51}_{-0.47}$	$0.57^{+0.09}_{-0.12}$	7.02/5	1.58
2MASXi J0729087 +400836	2002	$1.35^{+0.14}_{-0.14}$	$3.74^{+0.26}_{-0.24}$	53.75/65	0.71
RBS 874	1891	$1.53^{+0.12}_{-0.12}$	$1.01^{+0.05}_{-0.06}$	50.76/60	1.39
PG 1302–102	2379	$1.59^{+0.13}_{-0.12}$	$2.00^{+0.12}_{-0.10}$	51.56/64	1.66
FBQS J163302.6 +234928	1388	$1.73^{+0.13}_{-0.12}$	$1.35^{+0.08}_{-0.07}$	57.76/56	1.55
Mrk 504	2093	$1.59^{+0.18}_{-0.17}$	$3.90^{+0.27}_{-0.34}$	57.01/48	1.30
4C +50.43	580	$1.74^{+0.21}_{-0.20}$	$0.26^{+0.03}_{-0.03}$	20.52/25	1.56

Notes. DOF stands for "degrees of freedom." Error bars represent 90% confidence intervals.
[a] Total counts in the observed 0.5–8 keV band.
[b] Fit in the rest-frame 2–10 keV band.
[c] Flux in the rest-frame 2–10 keV band, in units of 10^{-12} erg cm^{-2} s^{-1}.

Graham et al. (2015b) had a suspiciously low mass listed for 2MASXi J0729087+400836, $\log(M_{\rm BH}/M_\odot) = 5.71$, leading to a suspiciously high Eddington ratio. We instead use the mass from Oh et al. (2015) for this source. Assuming that these single-epoch SMBH masses represent the total binary mass,[13] we calculated separations for each binary SMBH assuming circular orbits and a mass ratio $q = M_2/M_1 = 0.5$ where $M_{1,2}$ are the masses of the two SMBHs. The separations are expressed in terms of the gravitational radius r_g, where $r_g = GM/c^2$, G is the gravitational constant, M is the total binary mass, and c is the speed of light.

There is a well-established correlation between X-ray spectral index Γ and the Eddington ratio of AGNs, $\lambda_{\rm Edd} = L_{\rm bol}/L_{\rm Edd}$, where $L_{\rm bol}$ is the bolometric luminosity and $L_{\rm Edd}$ is the Eddington luminosity (Trakhtenbrot et al. 2017). In addition, AGN variability correlates with the Eddington ratio (Guo & Gu 2014; Rumbaugh et al. 2018). Sources with lower Eddington ratios have harder X-ray spectra and are more variable. As it may have implications for this work, we estimated the Eddington ratios for the sample. Bolometric luminosities were estimated using the 2–10 keV bolometric correction $\kappa_x = L_{\rm bol}/L_X$, where L_X is the rest-frame 2–10 keV X-ray luminosity. L_X was calculated using our measured values of f_{2-10} (listed in Table 2) and the luminosity distance for each source listed in the NASA/IPAC Extragalactic Database (NED). A value of $\kappa_x = 23$, the median bolometric correction for unobscured AGNs (Lusso et al. 2011), was used to derive the bolometric luminosity. Finally, the bolometric luminosities were divided by the Eddington luminosity for each object, which was estimated using $L_{\rm Edd} = 1.26 \times 10^{38}\,(M_{\rm BH}/M_\odot)$ erg s^{-1}.

The CRTS quasars vary widely in their binary properties, with SMBH masses ranging from $4.9 \times 10^6\,M_\odot$ to $7.2 \times 10^9\,M_\odot$ and binary separations ranging from $57\,r_g$ to more than $8400\,r_g$. They generally have typical quasar Eddington ratios of a few tenths, with the exception of 4C +50.43, which has an Eddington ratio of ≈2 according to our methodology. However, 4C +50.43 is radio loud, and radio-loud quasars are known to have elevated X-ray emission (e.g., Zamorani et al. 1981; Miller et al. 2011), implying that 4C +50.43 is unlikely to be super-Eddington. All the other sources in our sample are radio quiet, with radio fluxes several orders of magnitude lower than 4C +50.43.

These properties, as well as the observed period from CRTS and galaxy morphology, are listed in Table 3. The morphologies are based on visual inspection of Pan-STARRS images, supplemented by SDSS images when available. Five of the sources appear unresolved in the ground-based imaging, with the AGN outshining the host galaxy. The two lowest redshift sources show a bright, compact nucleus within a disk-like host galaxy. The table cites published literature that discusses the morphologies of two of the galaxies, both of which show morphological evidence of recent merger activity.

3.2. X-Ray Spectral Indices

Several of the theoretical models discussed in Section 1.2 predict that merging SMBH systems should have harder X-ray spectra than isolated accreting SMBHs. We therefore first analyzed the X-ray spectra to determine if the candidate merging SMBH systems had unusual X-ray spectral indices. Table 2 presents the results from our fitting, showing that the spectral indices range from 1.35 to 2.29, with a mean value of 1.68 ± 0.27. Such a mean value is on the low (or hard) side for AGNs in general, which typically have $\Gamma \sim 1.9$, but not inconsistent with their full range of ∼1.5–2.0 (e.g., Nandra & Pounds 1994; Shemmer et al. 2008; Brightman et al. 2013).

To make this comparison more quantitative, we used a two-sample Kolmogorov–Smirnov (KS) test to compare the spectral indices of our sample with the spectral indices of accreting SMBHs in the BAT AGN Spectroscopic Survey (BASS; Ricci et al. 2017), using their tabulated values of $\Gamma_{0.3-10}$ in Table 15. PG 1302–102 was present in the BASS data set, so it was discarded from the BASS sample before the KS test was

[13] The masses were ultimately calibrated using broad-line reverberation relations derived from local Seyfert galaxies. As the extent of a quasar BLR is likely far larger than the subparsec SMBH binary separations considered here, taking the measured mass to be the total binary mass is reasonable within the caveat concerning the unclear extent to which the original relations apply to luminous quasars.

Table 3
SMBH Binary Properties, Based on Table 2 in Graham et al. (2015b)

Object	$\log M_{\rm BH}$ ($M_\odot$)	r (r_g)	Period (day)	$L_{\rm bol}/L_{\rm Edd}$	Morphology
2MASSi J0411469+132416	8.16	922	1851	0.18	unresolved; possible close neighbor
2MASXi J0729087+400836	7.74	1799	1612	0.18	nucleated galaxy
RBS 874	8.43	493	1515	0.50	unresolved
PG 1302–102	8.50	516	1694	0.30	unresolved; merger features (Hong et al. 2015)
FBQS J163302.6+234928	9.86	57	2040	0.12	unresolved
Mrk 504	6.69	8437	1408	0.46	nucleated ring galaxy (Buta 2017)
4C +50.43	8.18	677	1975	2.22	unresolved

Note. Masses are single-epoch mass measurements based on scaling relations for nonbinary AGNs and are assumed to be the total binary mass (e.g., $M_1 + M_2$; see text for details). Separations (r) assume mass ratios of $q = M_2/M_1 = 0.5$. Morphologies are based on PanSTARRS, supplemented with SDSS when available.

performed. The KS test resulted in a p-value of 0.272, which is too large to reject the null hypothesis that our source spectral indices were drawn from the same distribution as the BASS sample. Cutting the BASS sample to only include unobscured AGNs (i.e., with $N_{\rm H} < 10^{22}\,{\rm cm}^{-2}$) and AGNs with Eddington ratios similar to our sample ($0.1 < L/L_{\rm Edd} < 1$) resulted in a p value of 0.107, not changing the results of the KS test. Further cuts on the BASS control sample based on parameters such as SMBH mass and redshift are inadvisable as our sample is too heterogeneous for this to be warranted (see Tables 1 and 3). We therefore conclude that these seven candidate merging SMBH systems have X-ray colors, or spectral indices, typical of isolated quasars, at least over the observed 0.5–8 keV range probed by Chandra. To investigate spectral hardening at higher energies would require observations with a satellite sensitive to >10 keV photons, such as the Nuclear Spectroscopic Telescope Array (NuSTAR; Harrison et al. 2013).

3.3. Optical-to-X-Ray Luminosities

We next investigated whether the candidate merging SMBH systems had unusually strong (or weak) X-ray emission, as suggested by some theoretical models. For this analysis, we considered the relationship between the X-ray luminosity and UV/optical luminosity, as quantified by the $\alpha_{\rm OX}$ parameter (e.g., Tananbaum et al. 1979; Just et al. 2007; Lusso et al. 2010). The relation between the two quantities is typically expressed as a linear correlation $\log(L_{2\,\rm keV}) = \gamma\log(L_{2500\text{Å}})+\beta$ (Lusso & Risaliti 2016), or in terms of the parameter $\alpha_{\rm OX}$, defined as

$$\alpha_{\rm OX} = -\frac{\log(f_{2\,\rm kev}/f_{2500\text{Å}})}{2.605}. \quad (1)$$

The mean value for $\alpha_{\rm OX}$ is typically around 1.5 (e.g., Lusso & Risaliti 2016).

We recovered the monochromatic rest-frame 2 keV flux density from the XSPEC model. For the rest-frame 2500 Å flux density, we linearly interpolated between the two nearest effective wavelengths present in public archives of large surveys. For most of the sources, this was the far-UV (FUV) and near-UV (NUV) observations from the Galaxy Evolution Explorer (GALEX) All-Sky Imaging Survey (Bianchi et al. 2017), but for the higher-redshift sources FBQS J163302.6 +234928 and 4C +50.43, we used u- and g-band data from the SDSS and g- and r-band data from PanSTARRS, respectively. To correct for Galactic extinction, we used the Schlafly & Finkbeiner (2011) reddening map to determine $E(B-V)$ at the location of each source. For the SDSS and PanSTARRS photometry, we used the NED online extinction calculator to determine the implied extinction in the optical bands for the Fitzpatrick (1999) mean extinction curve. For the GALEX bands, we used the same NED extinction calculator to determine the CTIO V-band extinction and then converted this to GALEX FUV and NUV extinctions using the Fitzpatrick & Massa (1990) parameterization of the UV extinction curve.

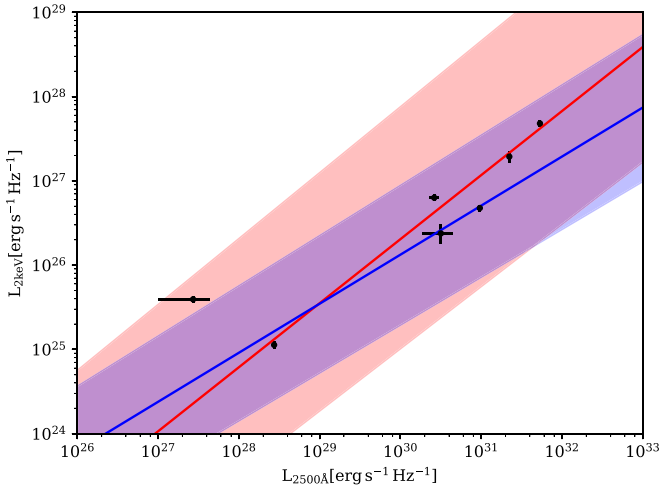

Figure 1. $L_{2500\text{Å}}$ vs. $L_{2\rm keV}$ for our seven sources. Error bars represent propagated 1σ uncertainties for optical fluxes and 90% confidence intervals for X-ray fluxes. In red is the relation from Equation (6) of Lusso et al. (2010) and in blue is the relation for the main sample from Table 2 of Lusso & Risaliti (2016). The shaded regions represent 1σ deviations from the mean relation.

We then computed the luminosity of each source at 2500 Å and 2 keV using the luminosity distances listed in NED for each source. Our calculated values of $\alpha_{\rm OX}$ for each source are listed in the final column of Table 2. The values range from 0.71 to 1.66, with a mean value of 1.39. Figure 1 plots $L_{2\rm keV}$ as a function of $L_{2500\text{Å}}$ for our sources, with the corresponding relations from Lusso et al. (2010) and Lusso & Risaliti (2016). Out of all the candidate binary SMBH systems investigated here, none are outside the error bars of Lusso et al. (2010) and only one (2MASXi J0729087+400836) is more than 1σ away from the mean trend line of Lusso & Risaliti (2016). We therefore conclude that these seven candidate merging SMBH systems have optical-to-X-ray luminosities typical of isolated AGNs, at least over the observed 0.5–8 keV range probed by Chandra.

4. Discussion

We find no obvious differences between the X-ray spectra of the seven subparsec binary quasar candidates in our sample and the X-ray spectra of the quasar population at large, at least over the energies observed by Chandra. However, the meaning of this result is unclear. Due to the small sample size studied, unless the differences between binary SMBH and single SMBH spectra are large, there is little chance of detecting a statistically significant difference between binary SMBH quasars and the larger quasar population. We first discuss how details of the binary SMBH models might affect the interpretation of our X-ray results (Section 4.1), and we then discuss potential concerns with the sample itself (Section 4.2).

4.1. Concerns with Binary SMBH Models

Assuming the models in the literature are correct, there are several reasons why our sources might truly be subparsec binary SMBH systems but we still would not have expected to observe differences between the Chandra spectra of our sources and single SMBH systems. The Roedig et al. (2014), Tang et al. (2018), and d'Ascoli et al. (2018) models of SMBH binaries have distinct peaks in their X-ray spectra outside the rest-frame 2–10 keV range of energies we observed for most sources, while Figure 3 of Roedig et al. (2014) and Figure 17 of Ryan & McFayden (2017) show only a very slight hardening of the X-ray spectra in the 2–10 rest-frame keV band. We note that the binary SMBH candidate PSO J334.2028+01.4075 (identified as a candidate by Liu et al. 2015) was observed by Foord et al. (2017) using Chandra, and no peculiarities in the X-ray spectrum were found.[14] It is therefore possible that the signatures of a binary SMBH lie outside the energy range of Chandra.

Farris et al. (2015a) found that the enhancement of emission in binary SMBH systems likely extends to energies lower than the soft X-ray band due to thermal emission from the accretion streams that thread the central cavity. If this emission is enhanced in binary SMBH systems relative to single SMBH systems across the entire optical–UV–X-ray range, then we might not expect our sources to have $\alpha_{\rm OX}$ values distinct from the larger quasar population.

The binary separations, a, are also likely an issue for this set of targets being compared to theoretical models. d'Ascoli et al. (2018) find that changing the separation of an SMBH binary alters the temperature ratio of the mini disks relative to the circumbinary disks, with implications for the high-energy spectra. Roedig et al. (2014) specifically highlight that their predicted excess thermal X-ray emission would only be clearly distinguishable from ordinary coronal X-rays for binary separations less than 100 gravitational radii, i.e., $<100\,r_g$. Many of the published models examine very tight subparsec binary systems. For example, d'Ascoli et al. (2018) modeled a binary with $a = 20\,r_g$, while Tang et al. (2018) start with a separation $a = 60\,r_g$ and evolve it to merger. Roedig et al. (2014), Ryan & McFayden (2017), and Farris et al. (2015a) considered wider binaries with $a \leqslant 300\,r_g$, $a \approx 100\,r_g$, and $a = 100\,r_g$, respectively. Farris et al. (2015b) started with a binary at around the same separation as Farris et al. (2015a) and evolved it until merger.

[14] Note, however, that recent work on PSO J334.2028+01.4075 has weakened the case for periodicity in its optical light curve (e.g., Liu et al. 2016) and disfavored its status as a binary SMBH system (e.g., Benke et al. 2019).

Considering the binary separations in Table 3, only one of our sources has a binary separation $a < 300\,r_g$ (FBQS J163302.6+234928), and two are separated by more than $1000\,r_g$ (2MASXi J0729087+400836 and Mrk 504). Therefore, it is possible that our sources indeed contain binary SMBHs, but with larger separations than what theorists have modeled to date and at separations where the X-ray spectra are largely indistinguishable from isolated SMBHs.

Furthermore, modeling the extreme regions around isolated accreting SMBHs has many uncertainties, such as the value of the disk viscosity, α, in the Shakura & Sunyaev (1973) accretion disk model (e.g., King et al. 2007), or understanding the geometry of the X-ray-emitting corona. Extending these simulations to binary quasars with relativistic velocities is clearly pushing the theoretical models to new, uncertain regimes. Many uncertainties in models of binary SMBHs arise due to simplifying assumptions. Numerical constraints mean modeled accretion disks are often thicker than AGN disks are in actuality. This shifts the disk Mach number and therefore the frequency of emitted radiation (Tang et al. 2018). Effectively, these simulated disks are much hotter than those in reality and so the thermal X-ray emission predicted in these simulations needs to be scaled down to lower photon energies.

Similarly, coronae, which are believed responsible for AGN X-ray emission through inverse Compton upscattering of thermal disk photons, are generally not modeled but are simply either painted on (e.g., d'Ascoli et al. 2018) or modeled as thermal emission (e.g., Farris et al. 2015a, 2015b; Tang et al. 2018). d'Ascoli et al. (2018) note that the manner in which they introduce the corona into their model would lead to an underestimate of hard inverse Compton X-rays and an overestimate of softer thermal X-rays, while Tang et al. (2018) note their lack of a true corona would overestimate the ability of the Doppler effect to suppress lower-energy X-rays. A first-principles description of AGN coronae is not present at this time, and models have difficulty generating observed SEDs even for single isolated SMBHs. This lack of understanding of the corona introduces complications for direct comparisons of the theoretical SEDs of binary SMBHs to the SED of a single SMBH. Finally, we note that most of the theoretical models use a fiducial SMBH mass of $10^8\,M_\odot$, while our sample ranges from 10^6 to $10^9\,M_\odot$. This likely has some implications in terms of the expected slope and peak energy of the disk emission. However, it should be noted that the dependence of the disk thermal emission on SMBH mass is not as strong as the dependence on binary separation and disk Mach number (e.g., Farris et al. 2015a, 2015b).

4.2. The True Nature of the Sources

It is uncertain whether or not the seven CRTS quasars in our sample are truly periodic sources. Quasars are known to vary stochastically. The power spectrum of these fluctuations is broad, with the power increasing at low frequencies ("red noise"). The spectrum is often approximated as a power law, $P(f) \propto f^{-\alpha}$, with $\alpha \gtrsim 1$ over long timescales (Vaughan 2013). It is possible for this noise to generate apparent periodicity when there is none; e.g., Vaughan et al. (2016) generated false periodicity in simulated CRTS light curves of PG 1302–102 even though the quasar's output was generated as a DRW or Gaussian noise. This can occur even for well-sampled data as long as the number of period cycles observed is small (Barth & Stern 2018). It is also the case that when searching for an effect

within a wide parameter space where the true location of the effect is unknown, statistically significant detections will happen by pure chance, the so-called "look-elsewhere effect" (Gross & Vitells 2010). Properly accounting for the false-alarm probability due to the look-elsewhere effect requires a noise model, and if the true stochastic variability contains more power than the best-fit DRW light curves, the purported periodicity can disappear with further observations.

The original Graham et al. (2015b) survey considered CRTS light curves for 243,500 quasars, looking for a strong Keplerian periodic signal with at least 1.5 cycles over a baseline of nine years. Though simulated data sets assuming stochastic variability (e.g., red noise) produced no equivalent candidates, implying a low likelihood of spurious detections, the short sampling time relative to the best-fit periods raises a natural concern for false positives.

In addition, even if the periodic behavior observed by CRTS is real, this does not necessarily mean that the quasars in our sample are all subparsec binaries. A hotspot on the accretion disk could produce a periodic light curve, with the caveat that many of the mechanisms that might produce a disk hotspot involve an SMBH binary (see D'Orazio et al. 2015a and references therein). There are alternative explanations for periodicity that involve only a single SMBH. For example, SMBHs are all expected to have nonzero angular momentum, and so Lense–Thirring precession will be important if the accretion disk is offset from the equatorial plane of the rotating black hole (Bardeen & Petterson 1975). This could cause both the relativistic jet and the inner accretion disk to precess and create periodic (or quasiperiodic) variability in the optical light curve. Frequent misalignments between the accretion disk and the black hole axis are theoretically expected to occur (Hopkins & Quataert 2010; Hopkins et al. 2012). Graham et al. (2015b), using the results of Ulubay-Siddiki et al. (2009) and Tremaine & Davis (2014), found that the precession period of a warped AGN disk is within an order of magnitude of the potential periods of our sources (assuming an SMBH mass of $10^8\,M_\odot$). However, the precession is damped on a timescale that is short compared to typical AGN lifetimes (Tremaine & Davis 2014; Graham et al. 2015b). Thus, Lense–Thirring precession in an AGN would be rarely observed.

Finally, and perhaps relatedly, the observed quasar periodicity might be caused by the same processes that cause quasiperiodic oscillations (QPOs) in black hole X-ray binaries (BHXBs—i.e., binary systems including a stellar-mass black hole; for a recent review of black hole QPOs, see Motta 2016). Graham et al. (2015b) noted that naively scaling the low-frequency ∼1 Hz QPO of the $\sim 12\,M_\odot$ microquasar GRS 1915 +105 (see Yan et al. 2013 and references therein) to the estimated mass of PG 1302–102 yields a QPO period that overlaps the observed periodicity of PG 1302–102's optical light curve. On the other hand, with the physics of QPOs still uncertain, and the wide range of frequencies spanned by low-frequency QPOs for a given source (Wijnands & Klis 1999), it is not clear that low-frequency QPOs scale linearly with black hole mass. As one example, Menou & Quataert (2001) note that ionization instabilities, one postulated source of QPOs in BHXBs, will be much more important for stellar-mass binary black holes than for SMBHs. In addition, we note that recent work shows that QPOs in BHXBs appear more associated with the inverse Compton X-ray emission from the corona and not with the thermal accretion disk component (e.g., Remillard & McClintock 2006; Ingram et al. 2009; Ingram & Done 2011). Quasars also have cooler accretion disks than BHXBs, with emission that peaks at rest-frame UV energies rather than the X-ray energies of BHXBs. Therefore, naively scaling the physics of QPOs from BHXBs to SMBHs might not produce periodic light curves at optical wavelengths.

4.3. Conclusions

We find no obvious differences between the X-ray spectra of the seven candidate subparsec binary SMBHs in our sample and the X-ray spectra of the quasar population at large, at least over the energies observed by Chandra. Many theoretical models predict differences in the X-ray spectra of close binary SMBHs, though the models have a wide range of predictions, and the models are not all consistent with each other. Furthermore, most of the models investigate binaries with closer separations than we estimate for our sample. This implies inconclusive results from our survey: the observed sample may or may not indeed be subparsec binary SMBH systems.

For future work, analyses at other wave bands might be useful, such as monitoring the UV/optical spectra of candidate binary SMBHs for kinematic variability and periodicity, and/or searching for the proposed UV/optical "notch" in the SED due to the inner gap in the circumbinary accretion disk (Roedig et al. 2014). Note, however, that more recent simulations have failed to recover that gap (e.g., Farris et al. 2015b; d'Ascoli et al. 2018). Several models predict that spectral hardening of binary SMBHs might lie at higher energies than the bands investigated by Chandra, so further investigations of candidate binary SMBH sources with NuSTAR are an enticing option. However, as some predicted signatures lie as far out as 100 keV (Roedig et al. 2014), it is unclear whether even NuSTAR will be able to detect them.

We thank the anonymous referee for a very thorough report, which has improved the paper. Support for this work was provided by the National Aeronautics and Space Administration (NASA) through Chandra Award Number 18700580 issued by the Chandra X-ray Center, which is operated by the Smithsonian Astrophysical Observatory for and on behalf of the NASA under contract NAS8-03060. The work of D.S. was carried out at the Jet Propulsion Laboratory, California Institute of Technology, under a contract with NASA. Z.H. acknowledges support from NSF grant 1715661 and NASA grants 80NSSC19K0149 and NNX17AL82G. M.J.G. and S.G.D. were supported in part by NASA grant 16-ADAP16-0232 and NSF grants AST-1413600, AST-1518308, and AST-1749235. D.J.D. acknowledges funding from the Institute for Theory and Computation Fellowship. K.E.S.F. and B.M. were supported by NSF grant 1831412. H.D.J. was supported by the Basic Science Research Program through the National Research Foundation of Korea, funded by the Ministry of Education (NRF-2017R1A6A3A04005158).

Appendix
X-Ray Spectra of Sample

We include X-ray spectra for the full sample here, including the best-fit models and resulting residuals (Figure A1).

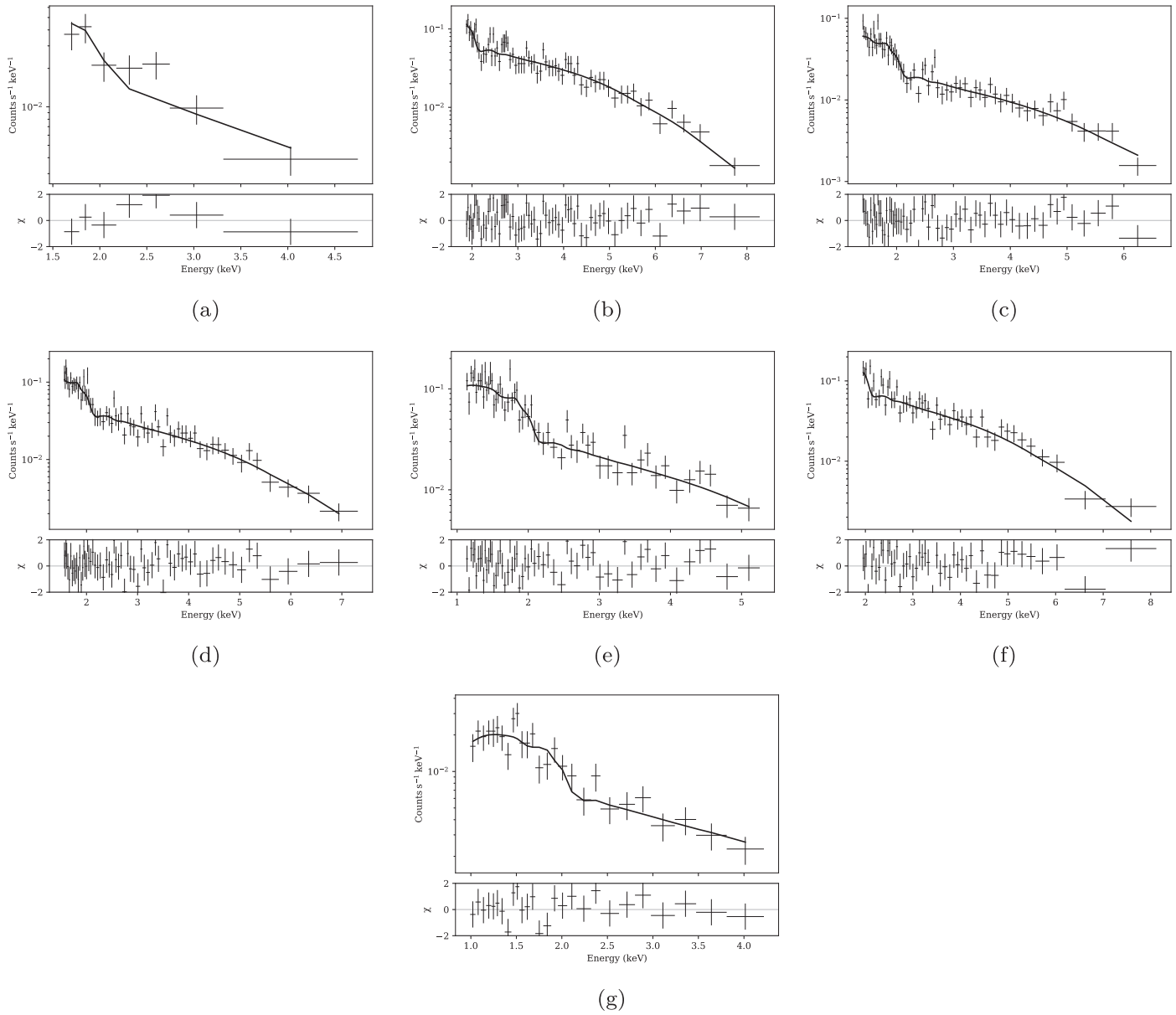

Figure A1. The Chandra X-ray spectra and best-fit models of the seven quasars in the sample. The quasars are (a) 2MASSi J0411469+132416, (b) 2MASXi J0729087+400836, (c) RBS 874, (d) PG 1302–102, (e) FBQS J163302.6+234928, (f) Mrk 504, and (g) 4C +50.43. The spectra are plotted over the rest-frame 2–10 keV band appropriate for each source's redshift. Error bars show 1σ confidence intervals.

ORCID iDs

M. Lynne Saade https://orcid.org/0000-0001-7163-7015
Daniel Stern https://orcid.org/0000-0003-2686-9241
Murray Brightman https://orcid.org/0000-0002-8147-2602
Zoltán Haiman https://orcid.org/0000-0003-3633-5403
S. G. Djorgovski https://orcid.org/0000-0002-0603-3087
Daniel D'Orazio https://orcid.org/0000-0002-1271-6247
Matthew J. Graham https://orcid.org/0000-0002-3168-0139
Hyunsung D. Jun https://orcid.org/0000-0003-1470-5901
Ralph P. Kraft https://orcid.org/0000-0002-0765-0511
Barry McKernan https://orcid.org/0000-0002-9726-0508
Alexei Vikhlinin https://orcid.org/0000-0001-8121-0234
Dominic J. Walton https://orcid.org/0000-0001-5819-3552

References

Amaro-Seoane, P., Audley, H., Babak, S., et al. 2017, arXiv:1702.00786
Artymowicz, P., & Lubow, S. H. 1994, ApJ, 421, 661
Bardeen, J. M., & Petterson, J. A. 1975, ApJL, 195, L65
Barth, A. J., Bennert, V. N., Canalizo, G., et al. 2016, ApJS, 217, 26
Barth, A. J., & Stern, D. 2018, ApJ, 859, 10
Begelman, M. C., Blandford, R. D., & Rees, M. J. 1980, Natur, 287, 307
Benke, P., Frey, S., & Gabányi, K. É 2019, in Proc. European VLBI Network Symp. 344, The Rise and Fall of a Binary AGN Candidate: The Story of PSO J334.2028+1.4075 (Trieste: SISSA), 98
Berczik, P., Merritt, D., Spurzem, R., & Bischof, H.-P. 2006, ApJL, 642, L21
Bianchi, L., Shiao, B., & Thilker, D. 2017, ApJS, 230, 24
Brightman, M., Silverman, J. D., Mainieri, V., et al. 2013, MNRAS, 433, 2485
Buta, R. J. 2017, MNRAS, 471, 4027
Caproni, A., Abraham, Z., & Monteiro, H. 2013, MNRAS, 428, 280
Charisi, M., Bartos, I., Haiman, Z., et al. 2016, MNRAS, 463, 2145
Comerford, J. M., Gerke, B. F., Stern, D., et al. 2012, ApJ, 753, 42
Comerford, J. M., Pooley, D., Barrows, R. S., et al. 2015, ApJ, 806, 219
Comerford, J. M., Schluns, K., Greene, J. E., et al. 2013, ApJ, 777, 64
d'Ascoli, S., Noble, S. C., Bowen, D. B., et al. 2018, ApJ, 865, 140
D'Orazio, D. J., Haiman, Z., Duffell, P., Farris, B. D., & MacFadyen, A. I. 2015a, MNRAS, 452, 2540
D'Orazio, D. J., Haiman, Z., & MacFayden, A. 2013, MNRAS, 436, 2997

D'Orazio, D. J., Haiman, Z., & Schiminovich, D. 2015b, Natur, 525, 351
D'Orazio, D. J., & Loeb, A. 2018, ApJ, 865, 185
D'Orazio, D. J., & Stefano, R. D. 2018, MNRAS, 474, 2975
de La Calle Pérez, I., Longinotti, A. L., Guainazzi, M., Bianchi, S., et al. 2010, A&A, 524, A50
De Rosa, L., Vignali, C., Bogdanović, T., et al. 2020, NewAR, 86, 101525
Dey, L., Valtonen, M. J., Gopakumar, A., et al. 2018, ApJ, 866, 11
Dickey, J. M., & Lockman, F. J. 1991, ARA&A, 28, 215
Dorn-Wallenstein, T., Levesque, E. M., & Ruan, J. J. 2017, ApJ, 850, 86
Drake, A. J., Mahabal, A., Beshore, E., et al. 2009, ApJ, 696, 870
Duffell, P. C., D'Orazio, D., Derdzinski, A., et al. 2019, arXiv:1911.05506
Eracleous, M., Boroson, T. A., Halpern, J., & Liu, J. 2012, ApJS, 201, 23
Farris, B. D., Duffel, P., MacFayden, A. I., & Haiman, Z. 2014, ApJ, 783, 134
Farris, B. D., Duffel, P., MacFayden, A. I., & Haiman, Z. 2015a, MNRAS, 446, L36
Farris, B. D., Duffel, P., MacFayden, A. I., & Haiman, Z. 2015b, MNRAS, 447, L80
Fitzpatrick, E. L. 1999, PASP, 111, 63
Fitzpatrick, E. L., & Massa, D. 1990, ApJS, 72, 163
Foord, A., Gültekin, K., Nevin, R., et al. 2020, ApJ, 892, 29
Foord, A., Gültekin, K., Reynolds, M., et al. 2017, ApJ, 851, 106
Fu, H., Myers, A. D., Djorgovski, S. G., et al. 2015, ApJ, 799, 72
Fu, H., Zhang, Z.-Y., Assef, R. J., et al. 2011, ApJL, 740, L44
George, I. M., & Fabian, A. C. 1991, MNRAS, 249, 352
Goulding, A. D., Pardo, K., Greene, J. E., et al. 2019, ApJL, 879, L21
Gower, A., Gregory, P. C., Hutchings, J. B., & Unruh, W. G. 1982, ApJ, 262, 478
Graham, M. J., Djorgovski, S. G., Stern, D., et al. 2015a, Natur, 518, 74
Graham, M. J., Djorgovski, S. G., Stern, D., et al. 2015b, MNRAS, 453, 1562
Gross, E., & Vitells, O. 2010, EPJC, 70, 525
Gualandris, A., Read, J. I., Dehnen, W., & Bortolas, E. 2017, MNRAS, 464, 2301
Guo, H., & Gu, M. 2014, ApJ, 792, 33
Guo, H., Liu, X., Shen, Y., et al. 2019, MNRAS, 482, 3288
Guo, H., Liu, X., Tayyaba, Z., & Liao, W.-T. 2020, MNRAS, 492, 2910
Haiman, Z. 2017, PhRvD, 96, 023004
Harrison, F. A., Craig, W. W., & Christensen, F. E. 2013, ApJ, 770, 103
Ho, L. C., Darling, J., & Greene, J. E. 2008, ApJS, 177, 103
Hong, J., Im, M., Kim, M., & Ho, L. C. 2015, ApJ, 804, 34
Hopkins, P. F., Hernquist, L., Hayward, C. C., et al. 2012, MNRAS, 425, 1125
Hopkins, P. F., & Quataert, E. 2010, MNRAS, 407, 1529
Hou, M., Liu, X., Guo, H., et al. 2019, ApJ, 882, 41
Ingram, A., & Done, C. 2011, MNRAS, 415, 2323
Ingram, A., Done, C., & Fragile, P. C. 2009, MNRAS, 397, L101
Ju, W., Greene, J. E., Rafikov, R. R., et al. 2013, ApJ, 777, 44
Jun, H., Im, M., Lee, H. M., et al. 2015, ApJ, 806, 109
Jun, H. D., Stern, D., Graham, M. J., et al. 2015, ApJL, 812, L12
Just, D. W., Brandt, W. N., Shemmer, O., et al. 2007, ApJ, 665, 1004
Kaastra, J. S., & Roos, N. 1992, A&A, 254, 96
Kharb, P., Lal, D. V., & Merritt, D. 2017, NatAs, 1, 727
King, A. R., Pringle, J. E., & Livio, M. 2007, MNRAS, 376, 1740
Komossa, S., Burwitz, V., Hasinger, G., et al. 2003, ApJL, 582, L15
Koss, M., Mushotzky, R., Treister, E., et al. 2011, ApJL, 735, L42
Koss, M., Mushotzky, R., Treister, E., et al. 2012, ApJL, 746, L22
Krause, M. G. H., Shabala, S. S., Hardcastle, M. J., et al. 2019, MNRAS, 482, 240
Kun, E., Gabányi, K. É, Karouzos, M., et al. 2014, MNRAS, 445, 1370
Kushwaha, P., Gupta, A. C., Wiita, P. J., et al. 2018, MNRAS, 479, 1672
Lehto, H. J., & Valtonen, M. J. 1996, ApJ, 460, 207
Li, Y.-R., Wang, J.-M., Ho, L. C., et al. 2016, ApJ, 822, 4
Liu, J., Eracleous, M., & Halpern, J. P. 2016, ApJ, 817, 42
Liu, T., Gezari, M., & Miller, M. C. 2018, ApJL, 859, L12
Liu, T., Gezari, S., Ayers, M., et al. 2019, ApJ, 884, 36
Liu, T., Gezari, S., Burgett, W., et al. 2016, ApJ, 833, 6
Liu, T., Gezari, S., Heinis, S., et al. 2015, ApJL, 803, L16
Liu, X., Shen, Y., Bian, F., et al. 2014, ApJ, 789, 140
Liu, X., Shen, Y., & Strauss, M. 2011, ApJL, 736, L7
Lobanov, A. P., & Roland, J. 2005, A&A, 431, 831
Lobanov, A. P., & Zensus, J. A. 2001, Sci, 294, 128
Lusso, E., Comastri, A., Vignali, C., et al. 2010, A&A, 512, A34
Lusso, E., Comastri, A., Vignali, C., et al. 2011, A&A, 534, A110
Lusso, E., & Risaliti, G. 2016, ApJ, 819, 154
Marscher, A. P., & Jorstad, S. G. 2011, ApJ, 729, 26
Mayer, L., Kazantzidis, S., Madau, P., et al. 2007, Sci, 316, 1874
McKernan, B., Ford, K. E. S., Kocsis, B., & Haiman, Z. 2013, MNRAS, 432, 1468
Menou, K., & Quataert, E. 2001, ApJ, 552, 204
Miller, B. P., Brandt, W. N., Shcneider, D. P., et al. 2011, ApJ, 726, 20
Motta, S. E. 2016, AN, 337, 398
Müller-Sánchez, F., Comerford, J. M., Nevin, R., et al. 2015, ApJ, 813, 103
Nandra, K., & Pounds, K. A. 1994, MNRAS, 268, 405
Nguyen, K., & Bogdanovic, T. 2016, ApJ, 828, 68
Nguyen, K., Bogdanovic, T., Runnoe, J. C., et al. 2019, ApJ, 870, 16
Oh, K., Yi, S. K., Schawinski, K., et al. 2015, ApJS, 219, 1
Pal, M., Kushwaha, P., Dewangan, G. C., & Pawar, P. K. 2020, ApJ, 890, 47
Pfeifle, R. W., Satyapal, S., Manzano-King, C., et al. 2019a, ApJ, 883, 167
Pfeifle, R. W., Satyapal, S., Secrest, N. J., et al. 2019b, ApJ, 875, 117
Qian, S. J., Britzen, S., Witzel, A., et al. 2018, A&A, 615, A123
Rafikov, R. 2016, ApJ, 827, 111
Remillard, R. A., & McClintock, J. E. 2006, ARA&A, 44, 49
Ricci, C., Trakhtenbrot, B., Koss, M. J., et al. 2017, ApJS, 233, 17
Rodriguez, C., Taylor, G. B., Zavala, R. T., et al. 2006, ApJ, 646, 49
Roedig, C., Krolik, J. H., & Miller, M. C. 2014, ApJ, 785, 115
Romero, G. E. 1995, Ap&SS, 234, 49
Rubinur, K., Das., M., & Kharb, P. 2019, MNRAS, 484, 4933
Rumbaugh, N., Shen, Y., Morganson, E., et al. 2018, ApJ, 854, 160
Ryan, G., & McFayden, A. 2017, ApJ, 835, 199
Ryu, T., Perna, R., Haiman, Z., et al. 2018, MNRAS, 473, 3410
Sandrinelli, A., Covino, S., Dotti, M., et al. 2016, ApJ, 151, 54
Satyapal, S., Secrest, N. J., Ricci, C., et al. 2017, ApJ, 848, 126
Schlafly, E. F., & Finkbeiner, D. P. 2011, ApJ, 737, 103
Severgnini, P., Cicone, C., Ceca, R. D., et al. 2018, MNRAS, 479, 3804
Shakura, N., & Sunyaev, R. A. 1973, A&A, 24, 337
Shemmer, O., Brandt, W. N., Maiolino, R., & Kaspi, S. 2008, ApJ, 682, 81
Shen, Y., Liu, X., Loeb, A., & Tremaine, S. 2013, ApJ, 775, 49
Shen, Y., & Loeb, A. 2010, ApJ, 725, 249
Shi, J.-M., & Krolik, J. H. 2015, ApJ, 807, 131
Tananbaum, H., Avni, Y., Branduardi, G., et al. 1979, ApJL, 234, L9
Tang, Y., Haiman, Z., & MacFayden, A. 2018, MNRAS, 476, 2249
Trakhtenbrot, B., Ricci, C., Koss, M. J., et al. 2017, MNRAS, 470, 800
Tremaine, S., & Davis, S. W. 2014, MNRAS, 441, 1408
Tsai, C.-W., Jarrett, T. H., Stern, D., et al. 2013, ApJ, 779, 41
Ulubay-Siddiki, A., Gerhard, O., & Arnaboldi, M. 2009, MNRAS, 398, 535
Valtonen, M. J., Ciprini, S., & Lehto, H. J. 2012, MNRAS, 427, 77
Valtonen, M. J., Lehto, H. J., Nilsson, K., et al. 2008, Natur, 452, 851
Vaughan, S. 2013, RSPTA, 371, 1984
Vaughan, S., Uttley, P., Markowitz, A. G., et al. 2016, MNRAS, 461, 3145
Voges, W., Aschenbach, B., Boller, Th., et al. 1999, A&A, 349, 389
Volonteri, M., Haardt, F., & Madau, P. 2003, ApJ, 582, 559
Wang, L., Greene, J. E., Ju, W., et al. 2017, ApJ, 834, 129
Wijnands, R., & Klis, M. V. D. 1999, ApJ, 514, 939
Xin, C., Charisi, M., Haiman, Z., et al. 2020, MNRAS, 496, 1683
Yan, S.-P., Ding, G.-Q., Wang, N., et al. 2013, MNRAS, 434, 59
Zamorani, G., Henry, J. P., Maccacaro, T., et al. 1981, ApJ, 245, 357